Characterization of the loss of plasmonic modes in planar metal–insulator–metal waveguides by a coupling-simulation approach

Chien-I Lin and Thomas K. Gaylord*

School of Electrical and Computer Engineering, Georgia Institute of Technology, Atlanta, Georgia 30332-0250, USA

*Corresponding author: tgaylord@ece.gatech.edu

Received 13 October 2009; accepted 12 January 2010;
posted 20 January 2010 (Doc. ID 118398); published 10 February 2010

Metal–insulator–metal (MIM) structures have been the subject of great interest as nanoscale plasmonic waveguides. The modeling and measurement of the loss in these waveguides is one of the critical issues in realizing the plasmon-based nanocircuitry. Due to the subwavelength size of the structure, the light injection and the measurement of the loss in MIM structures typically require tapered fibers or waveguides, as well as multiple waveguide structures with various length scales [8,9] or scanning near-field optical microscopy. The transverse transmission/reflection (TTR) method is presented for determining the loss of plasmonic modes in MIM waveguides. The approach is based on determining the width of the reflection angular spectrum in the attenuated total reflection configuration. Owing to its transverse character, the TTR method potentially provides a more straightforward and simpler way to determine the loss of plasmonic modes in MIM structures. © 2010 Optical Society of America

OCIS codes: 230.7370, 240.6680.

1. Introduction

During the past few years, surface plasmon (SP)-based waveguides have been the subject of intensive research [1–6]. Due to the nanometer-scale confinement and the "slow-wave" nature of SP [3–7], SP-based waveguides have been considered as promising candidates in realizing optical nanocircuitry. However, the loss in plasmonic waveguides is substantial owing to the intrinsic loss of the metal and is further magnified with enhanced transverse modal confinement [3–6], which is essential in integration of SP-based nanocircuitry. Therefore, the design, simulation, and measurement of the loss in plasmonic waveguides are critically important in the development of plasmonic waveguides.

The MIM structure is one of the most intensively investigated of plasmonic waveguides. Despite its larger loss compared with its complementary structure, the insulator–metal–insulator (IMI) plasmonic waveguide, the transverse modal size is significantly smaller in the former because of the relatively shallow field penetration to the skin depth of the metal cladding. Such small penetration also makes the MIM structures less sensitive to interface/surface defects, index mismatch of cladding layers, and crosstalk. However, the modal profile of a typical MIM structure is usually below the diffraction limit [3–5]. Therefore, the excitation and the loss measurement of an MIM plasmonic mode typically requires end-firing of tapered fibers or waveguides, as well as multiple waveguides structures with various length scales [8] or scanning near-field optical microscopy (SNOM) [10–12].

The transverse transmission/reflection (TTR) method [13] presented here may significantly simplify the loss measurement of the MIM plasmonic modes. Instead of conceptually injecting light from the end of the waveguides, e.g., finite-difference time-domain (FDTD) simulation [5,14,15], the TTR method excites a plasmonic mode in the transverse

0003-6935/10/060936-09$15.00/0

direction. This can be realized by making one of the metal cladding sufficiently thin (e.g., three to four skin depths) for light coupling. A high-index layer (e.g., prism) is then added adjacent to the thin metal layer to enable coupling. By plotting the fraction of power transmitted/reflected as a function of the normalized wave vector component of the incident wave, the Lorentzian maxima/minima are located at the real parts of the propagation constants, and the half-widths at half-maxima/minima (HWHM) of these resonances are equal to the imaginary parts of the propagation constants of the allowed plasmonic modes. Concisely stated, the TTR method provides a straightforward and simple approach for determining the complex propagation constants by simulating a coupled-waveguide structure. As a result, the TTR method has a similar configuration to the prism coupler introduced by Ulrich and Tien [16,17] and to the attenuated total reflection (ATR) configuration [18–20]. However, to the best of the authors' knowledge, this is the first time such configuration has been applied to the plasmonic modes in a MIM structure.

2. Formulation

A. TTR Method Formulation

The transfer matrix provides the basis for a systematic approach for analyzing multilayer structures, such as that shown in Fig. 1. For a transverse magnetic (TM) wave traveling in the $+z$ direction in the ith layer ($x_{i-1} \le x \le x_i$), the magnetic field is

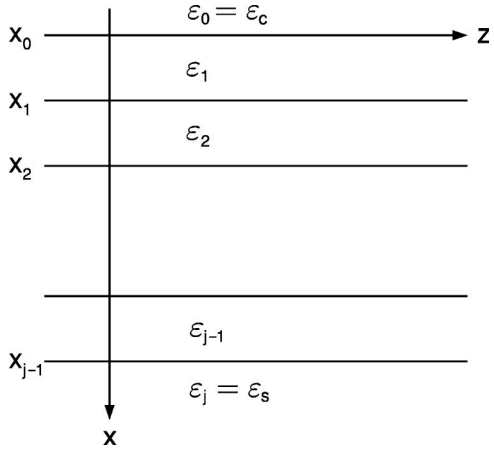

Fig. 1. Geometry of a multilayer structure.

$\vec{H}_i = \hat{y} H_{yi}(x) \exp[j(\omega t - \gamma z)]$, where $\hat{y}$ is the unit vector in the $+y$ direction and $\gamma = \beta - j\alpha$ is the complex propagation constant with β and α being the phase and attenuation propagation constants, respectively. The effective index N_{eff} is defined as $N_{\text{eff}} \equiv \beta/k_0$, where $k_0 = 2\pi/\lambda_0$ and λ_0 is the free space wavelength. The total magnetic field in the ith layer is the summation of $+x$ and $-x$ propagating waves, which can be expressed as

$$H_{yi}(x) = A_i \exp[-\kappa_{x,i}(x - x_{i-1})] + B_i \exp[+\kappa_{x,i}(x - x_{i-1})], \tag{1}$$

where A_i and B_i are the complex field amplitudes corresponding to the $+x$ and $-x$ propagating waves in the ith layer, respectively, $\kappa_{x,i} = (\gamma^2 - k_0^2 \varepsilon_i)^{1/2}$ is the complex transverse wave vector in the ith layer, and x_i defines the boundary between the ith and $(i+1)$th layers (Fig. 1). By matching the tangential components of the electric and magnetic fields at every interface, the field coefficient at the cover and the substrate can be related via the matrix equation

$$\begin{pmatrix} A_s \\ B_s \end{pmatrix} = M_{j-1} M_{j-2} \cdots M_1 M_0 \begin{pmatrix} A_c \\ B_c \end{pmatrix} = \begin{pmatrix} m_{11} & m_{12} \\ m_{21} & m_{22} \end{pmatrix} \begin{pmatrix} A_c \\ B_c \end{pmatrix}, \tag{2}$$

where the transfer matrix for the ith layer, M_i, is represented by

$$M_i = \frac{1}{2} \begin{pmatrix} \left(1 + f_i \frac{\kappa_{x,i}}{\kappa_{x,i+1}}\right) \exp(-\kappa_{x,i} d_i) & \left(1 - f_i \frac{\kappa_{x,i}}{\kappa_{x,i+1}}\right) \exp(\kappa_{x,i} d_i) \\ \left(1 - f_i \frac{\kappa_{x,i}}{\kappa_{x,i+1}}\right) \exp(-\kappa_{x,i} d_i) & \left(1 + f_i \frac{\kappa_{x,i}}{\kappa_{x,i+1}}\right) \exp(\kappa_{x,i} d_i) \end{pmatrix} \quad \text{for } i = 0, \cdots, j-1, \tag{3}$$

where for TE waves $f_i = 1$, while for TM waves $f_i = \varepsilon_{i+1}/\varepsilon_i$, and d_i is the thickness of the ith layer. By Eq. (2), the complex amplitude transmission and reflection coefficients are represented as

$$\text{cover incidence } (B_s = 0): \begin{pmatrix} t_s \\ 0 \end{pmatrix} = \begin{pmatrix} m_{11} & m_{12} \\ m_{21} & m_{22} \end{pmatrix} \begin{pmatrix} 1 \\ r_c \end{pmatrix}, \tag{4}$$

$$\text{substrate incidence } (A_c = 0): \begin{pmatrix} r_s \\ 1 \end{pmatrix} = \begin{pmatrix} m_{11} & m_{12} \\ m_{21} & m_{22} \end{pmatrix} \begin{pmatrix} 0 \\ t_c \end{pmatrix}. \tag{5}$$

By algebraic manipulation,

$$r_c = -\frac{m_{21}}{m_{22}}, \qquad r_s = \frac{m_{12}}{m_{22}}, \qquad t_c = \frac{1}{m_{22}}, \qquad t_s = \frac{m_{11}m_{22} - m_{12}m_{21}}{m_{22}}. \tag{6}$$

The fraction of the power reflected is

$$R_c = |r_c|^2, \qquad R_s = |r_s|^2. \tag{7}$$

The fraction of the power transmitted is

$$T_c = T_s = |t_c|^2 \frac{\kappa_c}{\kappa_s}\frac{\varepsilon_s}{\varepsilon_c} = |t_s|^2 \frac{\kappa_s}{\kappa_c}\frac{\varepsilon_c}{\varepsilon_s}. \tag{8}$$

By Eqs. (6) and (8) we can also obtain

$$m_{11}m_{22} - m_{12}m_{21} = \frac{\kappa_c}{\kappa_s}\frac{\varepsilon_s}{\varepsilon_c}. \tag{9}$$

The γ that makes the transmission and reflection coefficient infinite corresponds to the propagation constant of a guided or leaky mode of the waveguide structure [21].

The essence of the TTR method is based on expressing the fraction of the power transmitted approximately as a rational function of the poles of the complex propagation constants γ_l for leaky modes and lossy modes [13,22]. That is,

$$T = \left|\frac{1}{m_{22}}\right|^2 \frac{\kappa_c}{\kappa_s}\frac{\varepsilon_s}{\varepsilon_c} \simeq U(\beta)\left|\frac{1}{\prod_{l=1}^{M_p}(\beta - \gamma_l)}\right|^2, \tag{10}$$

where $U(\beta)$ is a slowly varying function of β and M_p is the number of poles. The γ_l values that make the transmission coefficients infinite correspond to the propagation constant of a guided or leaky mode of the waveguide structure. This is consistent with guided modes and leaky modes being solutions of $m_{22} = 0$. Given that $U(\beta)$ varies sufficiently slowly with β, the $T(\beta)$ has Lorentzian-type peaks located at $\beta = \mathrm{Re}(\gamma_l)$ and has HWHM values equal to $\alpha = \mathrm{Im}(\gamma_l)$. In the case that all the layers have zero or negligible loss, i.e., $|\mathrm{Im}(\varepsilon)| \ll |\mathrm{Re}(\varepsilon)|$, the fraction of power reflected can be approximated as $R = 1 - T$ [13]. Therefore the $R(\beta)$ have Lorentzian-type minima at $\beta = \mathrm{Re}(\gamma_l)$ and have HWHM $= \alpha = \mathrm{Im}(\gamma_l)$.

B. SP at a Single Metal/Dielectric Interface

Consider the structure shown in Fig. 2(a), which is a typical Otto configuration [23]. The SP is excited at the metal/dielectric interface by frustrated total internal reflection of the light incident upon the prism. The dispersion relation of the SP at a single metal/dielectric is given by

$$\beta_{\mathrm{SP}} = k_0\left(\frac{\varepsilon_m\varepsilon_d}{\varepsilon_m + \varepsilon_d}\right)^{1/2}, \tag{11}$$

which also implies that $\beta_{\mathrm{SP}} > \varepsilon_d^{1/2}k_0$ and that such SP mode exists only when $|\varepsilon_m| > -\varepsilon_d$, ignoring the typically small imaginary parts that lead to loss.

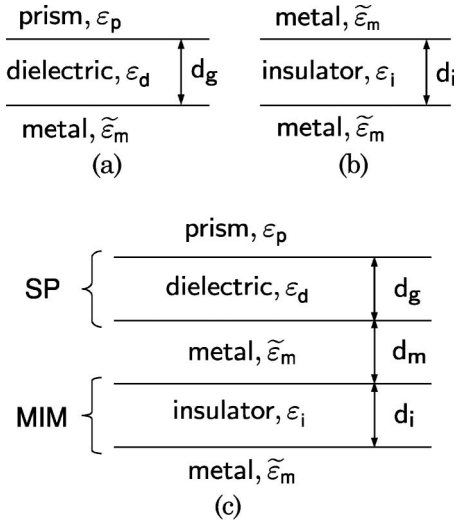

Fig. 2. (a) Schematic diagram of a single metal/dielectric interface-SP structure (Otto configuration). (b) Schematic diagram of a symmetric MIM structure. (c) Schematic diagram of a prism-loaded MIM structure.

However, in the Otto configuration, the thickness of the dielectric is not infinite, so part of the energy in the SP mode at the metal/dielectric interface can be coupled back into the prism. Therefore, the SP mode supported by the Otto configuration is perturbed by this leakage loss, which grows with decreasing gap dielectric thickness d_g. The propagation constant γ_{SP} of the perturbed SP mode can be obtained by solving the transfer matrix. The transfer matrix of this structure [Fig. 2(a)] is defined as

$$M_{\mathrm{SP}} = \begin{pmatrix} m'_{11} & m'_{12} \\ m'_{21} & m'_{22} \end{pmatrix}_{\mathrm{SP}}, \tag{12}$$

and the reflection coefficient is

$$r_{c,\mathrm{SP}} = -\frac{m'_{21}}{m'_{22}}. \tag{13}$$

The propagation constant γ_{SP} is the solution of $m'_{22} = 0$. As d_g decreases, the loss of the SP mode increases and the width of the fraction of power reflected $R_{c,\mathrm{SP}} = |r_{c,\mathrm{SP}}|^2$ increases, and the center of the $R_{c,\mathrm{SP}}$ resonance moves from β_{SP} to higher β. Example cases are illustrated in Section 3.

C. SP in MIM Structures

Figure 2(b) shows a symmetric MIM structure. There are two possible plasmonic modes in such a structure, one symmetric and one antisymmetric. The dispersion relations of the two modes are given by

$$\text{symmetric: } \tanh\left(\frac{\kappa_i d_i}{2}\right) = -\frac{\kappa_m}{\kappa_i}\frac{\varepsilon_i}{\varepsilon_m}, \tag{14}$$

$$\text{antisymmetric: } \tanh\left(\frac{\kappa_i d_i}{2}\right) = -\frac{\kappa_i}{\kappa_m}\frac{\varepsilon_m}{\varepsilon_i}, \tag{15}$$

where d_i is the thickness of the insulator. The symmetric mode has no cutoff frequency. There is a symmetric mode for any frequency above zero frequency. The antisymmetric mode has a cutoff frequency at which the mode makes a transition between oscillatory (inside the metal) mode to a plasmonic mode [24,25]. It should be noted that β_s of the symmetric mode (TM_0) is always larger than β_{SP} of the metal/insulator interface, while β_a of the antisymmetric mode (TM_1) is always smaller than β_{SP}. In this study, only the TM_0 mode is of interest.

The propagation constants γ_{MIM} of the TM_0 modes can also be obtained by solving the transfer matrix. The transfer matrix of the MIM structure [Fig. 2(b)] is defined as

$$M_{MIM} = \begin{pmatrix} m_{11} & m_{12} \\ m_{21} & m_{22} \end{pmatrix}_{MIM}, \tag{16}$$

and the reflection coefficient is

$$r_{c,MIM} = -\frac{m_{21}}{m_{22}}. \tag{17}$$

The propagation constants γ_{MIM} are the solutions of $m_{22} = 0$. It should be noted that the plasmonic modes cannot be directly excited from the metal cladding. Therefore, $r_{c,MIM}$ does not have a physically achievable value (e.g., $|r_{c,MIM}| > 1$) near the resonances corresponding to the plasmonic modes. In this study, one side of the metal is made to be sufficiently thin for light coupling. A high-index layer, such as prism, is added adjacent to the thin metal layer to enable light coupling with a higher longitudinal wave vector. Detailed analysis on the prism-loaded MIM structure is provided in Subsection 2.D.

D. Prism-Loaded MIM Structure

Based on the transfer matrix formulation, the prism-loaded MIM structure in Fig. 2(c) can be analyzed. The transfer matrix for this structure can be represented as

$$\begin{aligned} M &= \begin{pmatrix} m_{11} & m_{12} \\ m_{21} & m_{22} \end{pmatrix}_{MIM} \begin{pmatrix} \exp(-\kappa_m d_m) & 0 \\ 0 & \exp(\kappa_m d_m) \end{pmatrix} \begin{pmatrix} m'_{11} & m'_{12} \\ m'_{21} & m'_{22} \end{pmatrix}_{SP} \\ &= \begin{pmatrix} m_{12}m'_{21}\exp(\kappa_m d_m) + m_{11}m'_{11}\exp(-\kappa_m d_m) & m_{12}m'_{22}\exp(\kappa_m d_m) + m_{11}m'_{12}\exp(-\kappa_m d_m) \\ m_{22}m'_{21}\exp(\kappa_m d_m) + m_{21}m'_{11}\exp(-\kappa_m d_m) & m_{22}m'_{22}\exp(\kappa_m d_m) + m_{21}m'_{12}\exp(-\kappa_m d_m) \end{pmatrix}. \end{aligned} \tag{18}$$

Therefore, the reflection coefficient for the light incident at the prism is

$$r_c = -\frac{M(2,1)}{M(2,2)} = -\frac{m'_{21}}{m'_{22}}\frac{1 + \frac{m_{21}m'_{11}}{m_{22}m'_{21}}\exp(-2\kappa_m d_m)}{1 + \frac{m_{21}m'_{12}}{m_{22}m'_{22}}\exp(-2\kappa_m d_m)} = -\frac{m'_{21}}{m'_{22}}\left[1 + \frac{\frac{m_{21}}{m_{22}}\frac{m'_{11}m'_{22} - m'_{12}m'_{21}}{m'_{22}m'_{21}}\exp(-2\kappa_m d_m)}{1 + \frac{m_{21}m'_{12}}{m_{22}m'_{22}}\exp(-2\kappa_m d_m)}\right]. \tag{19}$$

In the case that $(m_{21}m'_{12})/(m_{22}m'_{22})\exp(-2\kappa_m d_m) \ll 1$, and using $m_{22} \simeq C \cdot (\beta - \gamma_{MIM})$ from Eq. (10), where C is a constant and $\gamma_{MIM} \equiv \beta_{MIM} - j\alpha_{MIM}$ is the complex propagation constant of the TM_0 mode in the MIM structure, Eq. (19) can be approximated as

$$\begin{aligned} r_c &\simeq -\frac{m'_{21}}{m'_{22}}\left[1 + \frac{m_{21}}{m_{22}}\frac{m'_{11}m'_{22} - m'_{12}m'_{21}}{m'_{22}m'_{21}}\exp(-2\kappa_m d_m)\right] \\ &= r_{c,SP}\left[1 + \frac{V(\beta)}{\beta - \gamma_{MIM}}\right], \end{aligned} \tag{20}$$

where the quantity $V(\beta) = m_{21}C(\kappa_p\varepsilon_m/\kappa_m\varepsilon_p)/(m'_{21}m'_{22}\exp(-2\kappa_m d_m))$, using $m'_{11}m'_{22} - m'_{12}m'_{21} = \kappa_p\varepsilon_m/\kappa_m\varepsilon_p$, is a slowly varying function of β. Based on Eq. (20), the fraction of power reflected $R_c = |r_c|^2$ can be expressed as

$$\begin{aligned} R_c &\simeq R_{c,SP}\left\{1 + 2 \cdot \mathrm{Re}\left[\frac{V(\beta)}{\beta - \gamma_{MIM}}\right]\right\} \\ &= R_{c,SP}\left\{1 + 2 \cdot \frac{(\beta - \beta_{MIM}) \cdot \mathrm{Re}[V(\beta)] + \alpha_{MIM} \cdot \mathrm{Im}[V(\beta)]}{(\beta - \beta_{MIM})^2 + \alpha_{MIM}^2}\right\}. \end{aligned} \tag{21}$$

Equation (21) shows that R_c is similar to $R_{c,SP}$, which has a resonance near the pole of m'_{22}, but R_c has one or more extra resonances that correspond to the plasmonic modes of the MIM structure near the poles of m_{22}. Equation (21) also implies that if the numerator of the second component is a negative constant [i.e., $V(\beta) = V\exp(3\pi/2)$, where V is a positive constant], $R_c/R_{c,SP}$ has a Lorentzian-type resonance centered at $N_{MIM} = \beta_{MIM}/k_0$ and a HWHM $= \alpha_{MIM}/k_0$. However, because $V(\beta)$ is not a constant and the phase of $V(\beta)$ is shifted due to the material loss in the metal, the HWHM of $R_c/R_{c,SP}$ is not precisely equal to α_{MIM}/k_0. Moreover, the approximation $(m_{21}m'_{12})/(m_{22}m'_{22})\exp(-2\kappa_m d_m) = 0$ made in Eq. (20) also causes errors since the metal thickness d_m is finite. The detailed error analysis of these errors is given in Appendix A,

and a step-by-step procedure for correcting for the errors is given in Appendix B.

3. Example Cases

In this section, the simulation performance and accuracy of the TTR method applied to various MIM structures is examined. The TTR simulation results are compared with rigorous results calculated by the argument principle method (APM) [26]. The first example chosen is a silver–air–silver structure with a 200 nm core at $\lambda = 0.6328\,\mu$m. The second example is a silver–oxide–silver structure with a 50 nm core at $\lambda = 1.55\,\mu$m. This structure has a relatively smaller core size and a higher β_{MIM}; therefore the gap between the prism and the MIM structure should be filled with high-index material (e.g., fluid) to facilitate the light coupling. More details are discussed in Subsection 3.B.

A. Silver–Air–Silver Structure

The first example is a symmetric MIM structure with a 200-nm void core and silver claddings. At the operating frequency $\lambda = 0.6328\,\mu$m, the silver has complex dielectric constant $\tilde{\varepsilon}_{Ag} = -15.9 - j1.07$, or equivalently, refractive index $\tilde{n}_{Ag} = 0.135 - j3.99$ [27]. The normalized propagation constant $\gamma_{\mathrm{MIM}}/k_0$ of the TM_0 mode calculated by APM is $1.13412 - j0.00505$, which corresponds to a loss of $0.44\,\mathrm{dB}/\mu$m or propagation length of $10\,\mu$m.

In order to apply the TTR method to this MIM structure, one of the silver claddings has to be sufficiently thin for light coupling and a high-index layer (e.g., prism) has to be placed adjacent to the thin silver cladding, as shown in Fig. 3. In this case, the skin depth of silver $\delta \sim 25$ nm, so d_m is chosen to be 75 nm and 100 nm to allow the appropriate coupling strength. The prism index n_p has to be sufficiently larger than N_{MIM} and is chosen to be 1.5.

The plane-wave reflection power spectra of the structure in Fig. 3 with $d_m = 100$ nm and $d_m = 75$ nm is plotted as functions of the effective index N_{eff} in Figs. 4 and 5, respectively, and summarized in Table 1. The effective index N'_{MIM} of the TM_0 mode is located at the minimum of the $R_c/R_{c,\mathrm{SP}}$ resonance, and the normalized attenuation coefficient $\alpha'_{\mathrm{MIM}}/k_0$ is equal to the HWHM, where the prime denotes results obtained by the TTR method, in contrast to the rigorous results obtained by APM. $R_{c,\mathrm{SP}}$ can be obtained by qualitatively subtracting out the TM_0 resonance from R_c for each d_a. It is shown in Table 1 that the results obtained by the TTR method are in good agreement with the rigorous result, especially in the case of $d_m = 100$ nm. The error in $\alpha'_{\mathrm{MIM}} < 5\%$ in the case of $d_m = 100$ nm and $\lesssim 10\%$ in the case of $d_m = 75$ nm. Larger d_m causes a smaller TM_0 resonance intensity and smaller perturbation, in agreement with the analysis of Subsection 2.D.

As described in Appendix A, the error in α'_{MIM} can be estimated. In the case of $d_m = 100$ nm, the error due to the finite thickness of the metal layer d_m is usually smaller than the half-resonance strength of $R_c/R_{c,\mathrm{SP}}$ as $d_a \to 0$, that is, $\lesssim 2\%$. Following the procedure described in Appendix B, the phase shift is fitted as $\Delta\phi_V \sim 15°$, and the normalized attenuation coefficient after correction is $\alpha''_{\mathrm{MIM}}/k_0 \sim 0.00515$. Similarly, in the case of $d_m = 75$ nm, the error due to finite d_m is $\lesssim 8\%$. The fitted $\Delta\phi_V \sim 15°$ and $\alpha''_{\mathrm{MIM}}/k_0 \sim 0.0051$. It is shown that in both cases, the α''_{MIM} values have less than 2% of error. It should be noted that no explicit information about d_a or d_m is needed in the correction procedure.

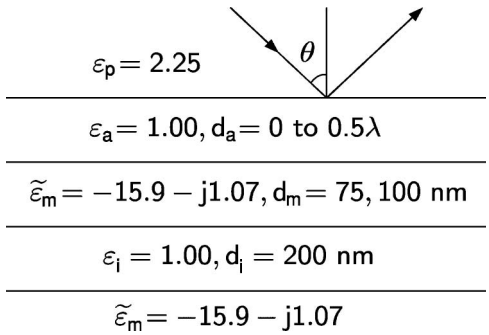

Fig. 3. Schematic diagram of the prism-loaded MIM structure with a 200 nm void core. The metal is silver with complex dielectric constant $\tilde{\varepsilon}_m = -15.9 - j1.07$, or equivalently refractive index $\tilde{n}_m = 0.135 - j3.99$ [27]. The operating wavelength is $0.6328\,\mu$m.

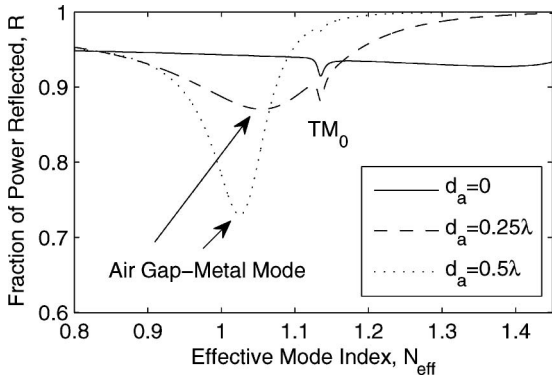

Fig. 4. Plane-wave reflection power spectrum of the structure in Fig. 3 with $d_m = 100$ nm. The x axis is the effective index $N_{\mathrm{eff}} \equiv \beta/k_0 = n_p \sin\theta$, and the y axis is the fraction of power reflected. The resonances corresponding to the air gap-metal plasmonic mode and the TM_0 mode of the MIM structure are labeled.

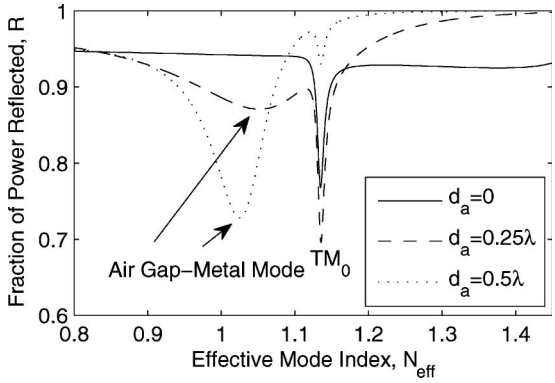

Fig. 5. Plane-wave reflection power spectrum of the structure in Fig. 3 with $d_m = 75$ nm.

Table 1. Normalized Complex Propagation Constant γ'_{MIM}/k_0 Calculated by the TTR Method, for the MIM Structure Shown in Fig. 3[a]

d_a	d_m	TTR Method
0	100 nm	$1.1348 - j0.0053$
0.25λ	"	$1.1350 - j0.0053$
0.50λ	"	$1.1348 - j0.0051$
0	75 nm	$1.1348 - j0.0055$
0.25λ	"	$1.1354 - j0.0057$
0.50λ	"	$1.1354 - j0.0053$

[a]The rigorous complex propagation constant for the TM_0 mode of the MIM structure without the prism loaded ($d_m = \infty$) is $\gamma_{MIM}/k_0 = 1.13412 - j0.00505$.

B. Silver–Oxide–Silver Structure

The second example is a symmetric MIM structure with a 50 nm SiO_2 core and silver claddings. At the operating frequency $\lambda = 1.55\,\mu$m, the silver has complex dielectric constant $\tilde{\varepsilon}_{Ag} = -86.6 - j8.74$, or equivalently, refractive index $\tilde{n}_{Ag} = 0.469 - j9.32$ [27]. The normalized propagation constant γ_{MIM}/k_0 of the TM_0 mode calculated by APM is $2.11140 - j0.02967$, which corresponds to a loss of 1.04 dB/μm or propagation length of 4.2 μm. The higher N_{MIM} in this case is the result of the higher index and smaller size of the core insulator.

In order to apply the TTR method to this structure, one of the silver claddings is made thinner and a prism is placed adjacent to the MIM structure. In this case, the skin depth of silver is $\delta \sim 26$ nm, so d_m is chosen to be 80 nm to allow the appropriate coupling strength. The prism index n_p is chosen to be 2.5.

The plane-wave reflection power spectrum of the structure in Fig. 6 is shown in Fig. 7 and summarized in Table 2. The N'_{MIM} and α'_{MIM} are obtained in the same manner as in the previous example. It is shown in Table 2 that the results of the TTR method are in good agreement with the rigorous result. The error in $\alpha'_{MIM} < 5\%$ for $d_f = 100$ and 200 nm and $<10\%$ for $d_f = 0$ and 50 nm.

Following Appendix A, the error of the HWHM can be estimated. The error due to finite d_m in this case is $\lesssim 6\%$. The fitted phase shift $\Delta\phi_V \sim 20°$, and the normalized attenuation coefficient after correction is $\alpha''_{MIM}/k_0 \sim 0.0297$. The detailed fitting procedure for this case is given in Appendix B.

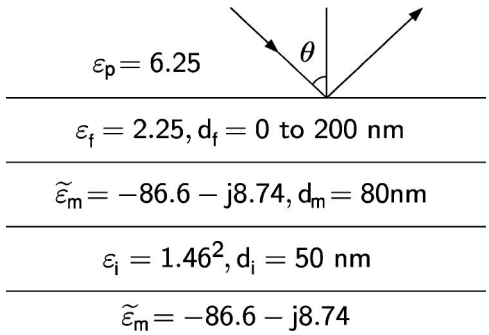

Fig. 6. Schematic diagram of the prism-loaded MIM structure with a 50 nm SiO_2 core. The metal is silver with complex dielectric constant $\tilde{\varepsilon}_m = -86.6 - j8.74$, or equivalently, refractive index $\tilde{n}_m = 0.469 - j9.32$ [27]. The operating wavelength is 1.55 μm.

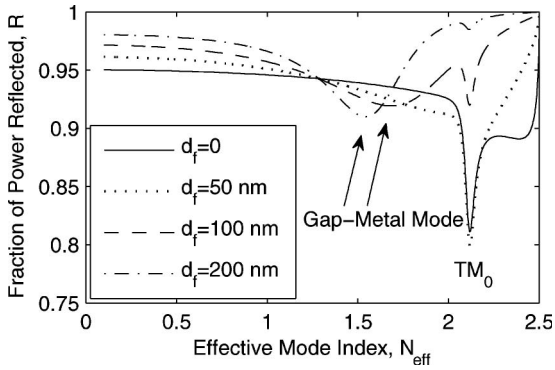

Fig. 7. Plane-wave reflection power spectrum of the structure in Fig. 6 with $d_m = 80$ nm.

4. Summary and Discussion

In this paper, a coupling simulation method, the transverse transmission/reflection (TTR) method, is presented for the characterization of the plasmonic modes in MIM structures. The TTR method is noteworthy for its simplicity and capability of characterizing plasmonic modes with a linkage to the physical attenuated total reflection (ATR) configuration. By simulating such a structure, both the real part and the imaginary part of the propagation constant of a plasmonic mode can be characterized by the angle and width of the Lorentzian-type reflection resonance. It is shown in the example cases that appropriate coupling strength can be obtained when the thickness of the metal is about three to four skin depths. The resulting errors in the attenuation coefficient are typically smaller than 10% and can be minimized using the analysis based on multiple reflection power spectra at various gap dielectric thickness.

To summarize, the TTR method presented here is a potentially powerful approach for characterizing plasmonic modes. Due to its transverse nature, a loss measurement based on the TTR method may obviate the need of tapered end-couplers and the need of multiple waveguide samples or scanning near-field optical microscopy (SNOM). A paper describing corresponding experimental results by the authors has recently been submitted for publication.

Table 2. Normalized Complex Propagation Constant γ'_{MIM}/k_0 Calculated by the TTR Method, for the MIM Structure Shown in Fig. 6[a]

d_f	d_m	TTR Method
0	80 nm	$2.1179 - j0.0326$
50 nm	"	$2.1191 - j0.0329$
100 nm	"	$2.1178 - j0.0305$
200 nm	"	$2.1167 - j0.0296$

[a]The rigorous complex propagation constant for the TM_0 mode of the MIM structure without the prism loaded ($d_m = \infty$) is $\gamma_{MIM}/k_0 = 2.11140 - j0.02967$.

$$\beta_{\mathrm{hm}} = \beta_{\mathrm{MIM}} + \alpha_{\mathrm{MIM}} \frac{-2\sin(\Delta\phi_V) \pm \{2[1+\cos(\Delta\phi_V)] + \sin^2(\Delta\phi_V)\}^{1/2}}{1+\cos(\Delta\phi_V)}, \tag{A3}$$

Appendix A: Detailed Error Analysis

The attenuation coefficient α'_{MIM} obtained from the TTR method is specified by the HWHM of $R_c/R_{c,\mathrm{SP}}$, which equals $\alpha'_{\mathrm{MIM}}/k_0$. Following Subsection 2.D, the quantity α'_{MIM} differs from the rigorously calculated attenuation coefficient α_{MIM}. The error in α'_{MIM} has three sources: (1) the finite metal thickness d_m, (2) the phase shift of $V(\beta)$ due to loss in the metal, and (3) the background variation in $V(\beta)$. A step-by-step procedure for obtaining the value of the attenuation coefficient α''_{MIM} corrected for these errors is given in Appendix B.

The first error is caused by the approximation $A \equiv (m_{21}m'_{12})/(m_{22}m'_{22})\exp(-2\kappa_m d_m) = 0$ in Eq. (20). Because of the m_{22} in the denominator, $|A|$ has a peak near where m_{22} has a pole, which is also near where $R_c/R_{c,\mathrm{SP}}$ has a minimum. In the worst case, the resonance strength of $R_c/R_{c,\mathrm{SP}}$ is decreased by $100|A|_{\max}\%$, and its HWHM is broadened by similar percentage. $|A|_{\max}$ can be estimated by comparing with the value of $(m_{21}/m_{22})[(m'_{11}m'_{22} - m'_{12}m'_{21})/(m'_{22}m'_{21})]\exp(-2\kappa_m d_m) = V(\beta)/(\beta - \gamma_{\mathrm{MIM}})$, which is the resonance strength of $R_c/R_{c,\mathrm{SP}}$. The transfer matrix M_{SP} when the gap dielectric thickness $d_g \to 0$ may be expressed as

$$M_{\mathrm{SP}}(d_g \to 0) = \frac{1}{2}\begin{pmatrix} 1+m'_{\mathrm{SP}} & 1-m'_{\mathrm{SP}} \\ 1-m'_{\mathrm{SP}} & 1+m'_{\mathrm{SP}} \end{pmatrix}, \tag{A1}$$

where $m'_{\mathrm{SP}} = (n_m^2\kappa_p)/(n_p^2\kappa_m)$, which is imaginary for a lossless metal. For a low-loss metal, $|(m'_{11}m'_{22} - m'_{12}m'_{21})/(m'_{22}m'_{21})| = |4m'_{\mathrm{SP}}/(1-m'^2_{\mathrm{SP}})|$ has values between 1 and 2 for $N_{\mathrm{eff}} = 0$ to $[n_m^2 n_p^2(n_m^2+n_p^2)/(n_m^4+n_p^4)]^1/2 \sim n_p$. Therefore, based on Eq. (21), the value of $|(m_{21}/m_{22})\exp(-2\kappa_m d_m)|$ is between 1/4 and 1/2 times the resonance strength of $R_c/R_{c,\mathrm{SP}}$ when $d_g \to 0$. Since the value of $|m'_{12}/m'_{22}|$ is between 1 and 2 for any d_g, $|A|_{\max}$ at any $d_g \lesssim 1/2$ times the resonance strength of $R_c/R_{c,\mathrm{SP}}$ when $d_g \to 0$. It should be noted that α'_{MIM} obtained without the approximation $A = 0$ [Eq. (19)] is always larger than that with the approximation [Eq. (20)].

The second source of error is caused by the material loss in the metal. In the case of a lossless metal, $\phi_V = 3\pi/2$. However, ϕ_V is shifted when the metal is lossy. Based on Eq. (21) and assuming $V(\beta) = V\exp[(3\pi/2) + \Delta\phi_V]$, where V is a positive constant, $\beta_{\min}$ at the minimum of the phase-shifted Lorentzian $R_c/R_{c,\mathrm{SP}}$ can be represented as

$$\beta_{\min} = \beta_{\mathrm{MIM}} + \alpha_{\mathrm{MIM}} \frac{\cos(\Delta\phi_V) - 1}{\sin(\Delta\phi_V)}, \tag{A2}$$

and β_{hm} values at the half-minimum points are where the positive and negative signs correspond to the right and left half-minimum points, respectively. Figures 8(a) shows the variation of $\beta_{\min}$ and β_{hm} values, and Fig. 8(b) shows the broadening effect of α'_{MIM} as a function of $\Delta\phi_V$.

The third source of error is caused by background variation of $V(\beta)$, and the effect is dependent on $\Delta\phi_V$. Assuming the phase-shifted Lorentzian is multiplied by a linearly varying function $V(\beta)$, Fig. 9 shows the variation of α'_{MIM} as a function of the percentage background variation, $|V(\beta_{\mathrm{MIM}} + \alpha_{\mathrm{MIM}})/V(\beta_{\mathrm{MIM}} - \alpha_{\mathrm{MIM}})| - 1$, at various $\Delta\phi_V$ values.

Appendix B: Method of Determining α''_{MIM}

Based on the discussion in Appendix A, the corrected α''_{MIM} can be obtained by using multiple R_c values at various d_g values, utilizing the fact that the variation of α'_{MIM} is proportional to the percentage background variation and that the slopes depend on the phase shift $\Delta\phi_V$ (Fig. 9). From the α'_{MIM} values obtained from the $V(\beta)$ variations, the quantity $\Delta\phi_V$ and the corrected α''_{MIM} can be estimated by the slope of the α'_{MIM} versus the percentage background variation. By definition, the variation of $|V(\beta)|$ is determined by the variation of $|(m'_{11}m'_{22} - m'_{12}m'_{21})/(m'_{22}m'_{21})|$ and $|(m_{21}/m_{22})\exp(-2\kappa_m d_m)|$; the former is related to the prism–dielectric–metal structure, and the latter is related to the MIM structure. Therefore, the variation of $|V(\beta)|$ can be controlled by varying the gap dielectric thickness d_g, while the variation of $|(m_{21}/m_{22})\exp(-2\kappa_m d_m)|$ stays constant and does not affect the slope of Fig. 9. The variation of $|(m'_{11}m'_{22} - m'_{12}m'_{21})/(m'_{22}m'_{21})|$ can be obtained by using

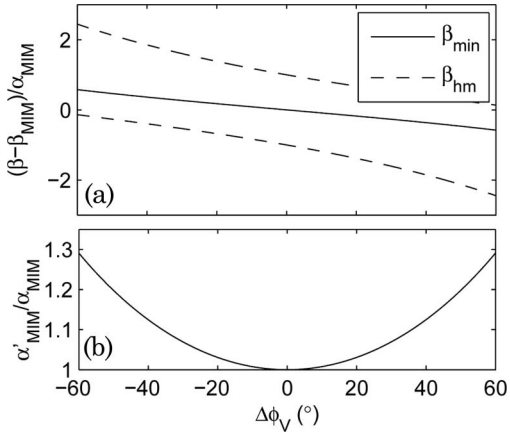

Fig. 8. (a) Variation of $\beta_{\min}$ and β_{hm} values as a function of the phase shift $\Delta\phi_V$ caused by the material loss of the metal. The upper β_{hm} corresponds to the right half-minimum point, and the lower one to the left half-minimum point. (b) Broadening of α'_{MIM} as a function of $\Delta\phi_V$.

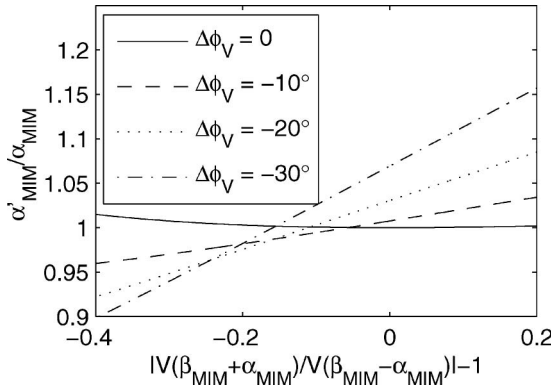

Fig. 9. Variation of α'_{MIM} as a function of the linear background variation at various phase shift $\Delta\phi_V$.

$$\left|\frac{m'_{11}m'_{22}-m'_{12}m'_{21}}{m'_{22}m'_{21}}\right|=\left|\frac{t_{s,\mathrm{SP}}t_{c,\mathrm{SP}}}{r_{c,\mathrm{SP}}}\right|\simeq T_{c,\mathrm{SP}}\propto 1-R_{c,\mathrm{SP}}, \tag{B1}$$

where $R_{c,\mathrm{SP}}$ can be obtained by qualitatively subtracting out the TM_0 resonance. It should be noted that no explicit information about d_f or d_m is needed, which means the correction procedure can be implemented by simply using multiple R_c values at various d_g values.

The correction procedure of α'_{MIM} is given by the following steps. For illustration purpose, the procedure is applied to the example case in Subsection 3.B.

1. Calculate/plot R_c versus N_{eff} at various d_f.
2. Produce $R_{c,\mathrm{SP}}$ versus N_{eff} by qualitatively subtracting out TM_0 resonance from R_c for each d_f.
3. From $R_c/R_{c,\mathrm{SP}}$ versus N_{eff}, estimate the error due to the finite d_m, which is the half-resonance strength as $d_f \to 0$. The error is ~6% in this case.
4. From $R_c/R_{c,\mathrm{SP}}$ versus N_{eff}, calculate β'_{MIM} from the location of the minimum and α'_{MIM} from the HWHM for each d_f. The quantity α'_{MIM} should be subtracted by the broadening error due to the finite d_m obtained in step 3.
5. From $R_{c,\mathrm{SP}}$ versus N_{eff} in step 2, calculate the background variation, $[1-R_{c,\mathrm{SP}}(\beta'_{\mathrm{MIM}}+\alpha'_{\mathrm{MIM}})]/[1-R_{c,\mathrm{SP}}(\beta'_{\mathrm{MIM}}-\alpha'_{\mathrm{MIM}})]-1$, for each d_f. The background variation is proportional to $|V(\beta'_{\mathrm{MIM}}+\alpha'_{\mathrm{MIM}})/V(\beta'_{\mathrm{MIM}}-\alpha'_{\mathrm{MIM}})|-1$ according to Eq. (B1). In this case, the background variation is ~4%, −3%, −27%, and −30% for $d_f = 0$, 50 nm, 100 nm, and 200 nm, respectively.
6. From the plot of α'_{MIM} versus the background variation (Fig. 10), estimate $\Delta\phi_V$ by comparing with Fig. 9. In this case, $\Delta\phi_V \sim 20°$.
7. Calculate the corrected attenuation α''_{MIM} from

$$\alpha''_{\mathrm{MIM}}=\frac{\alpha'_{\mathrm{MIM}}(\mathrm{Fig.\ 10})}{(\alpha'_{\mathrm{MIM}}/\alpha_{\mathrm{MIM}})(\mathrm{Fig.\ 9})}. \tag{B2}$$

In this case, $\alpha''_{\mathrm{MIM}}/k_0 \sim 0.0297$.

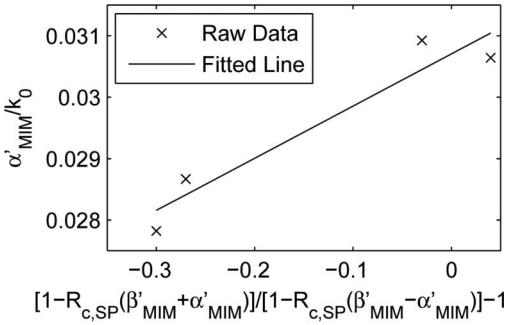

Fig. 10. Variation of α'_{MIM} as a function of the linear background variation for the example case in Subsection 3.B. β'_{MIM} and α'_{MIM} are obtained by using Table 2, while the latter is subtracted by the estimated broadening error due to finite d_m, which is ~6% in this case.

References

1. W. L. Barnes, A. Dereux, and T. W. Ebbesen, "Surface plasmon subwavelength optics," Nature **424**, 824–830 (2003).
2. S. I. Bozhevolnyi, V. S. Volkov, E. Devaux, J. Y. Laluet, and T. W. Ebbesen, "Channel plasmon subwavelength waveguide components including interferometers and ring resonators," Nature **440**, 508–511 (2006).
3. S. A. Maier, "Plasmonics: the promise of highly integrated optical devices," IEEE J. Sel. Top. Quantum Electron. **12**, 1671–1677 (2006).
4. E. Ozbay, "Plasmonics: merging photonics and electronics at nanoscale dimensions," Science **311**, 189–193 (2006).
5. E. Feigenbaum and M. Orenstein, "Modeling of complementary (void) plasmon waveguiding," J. Lightwave Technol. **25**, 2547–2562 (2007).
6. R. Zia, J. A. Schuller, A. Chandran, and M. L. Brongersma, "Plasmonics: the next chip-scale technology," Mater. Today **9**, 20–27 (2006).
7. H. Raether, *Surface Plasmons on Smooth and Rough Surfaces and on Gratings* (Springer-Verlag, 1988).
8. T. Goto, Y. Katagiri, H. Fukuda, H. Shinojima, Y. Nakano, I. Kobayashi, and Y. Mitsuoka, "Propagation loss measurement for surface plasmon-polariton modes at metal waveguides on semiconductor substrates," Appl. Phys. Lett. **84**, 852–854 (2004).
9. J. A. Dionne, H. J. Lezec, and H. A. Atwater, "Highly confined photon transport in subwavelength metallic slot waveguides," Nano Lett. **6**, 1928–1932 (2006).
10. U. Durig, D. W. Pohl, and F. Rohner, "Near-field optical-scanning microscopy," J. Appl. Phys. **59**, 3318–3327 (1986).
11. J. C. Weeber, Y. Lacroute, and A. Dereux, "Optical near-field distributions of surface plasmon waveguide modes," Phys. Rev. B **68**, 115401 (2003).
12. S. I. Bozhevolnyi, V. S. Volkov, E. Devaux, and T. W. Ebbesen, "Channel plasmon-polariton guiding by subwavelength metal grooves," Phys. Rev. Lett. **95**, 046802 (2005).
13. C.-I. Lin and T. K. Gaylord, "Attenuation and mode profile determination of leaky/lossy modes in multilayer planar waveguides by a coupling simulation method," Appl. Opt. **48**, 3603–3613 (2009).
14. G. Veronis and S. H. Fan, "Bends and splitters in metal-dielectric-metal subwavelength plasmonic waveguides," Appl. Phys. Lett. **87**, 131102 (2005).
15. Y. Matsuzaki, T. Okamoto, M. Haraguchi, M. Fukui, and M. Nakagaki, "Characteristics of gap plasmon waveguide with stub structures," Opt. Express **16**, 16314–16325 (2008).
16. R. Ulrich, "Theory of the prism-film coupler by plane-wave analysis," J. Opt. Soc. Am. **60**, 1337–1350 (1970).

17. P. K. Tien and R. Ulrich, "Theory of prism-film coupler and thin-film light guides," J. Opt. Soc. Am. **60**, 1325–1337 (1970).
18. A. E. Craig, G. A. Olson, and D. Sarid, "Experimental-observation of the long-range surface-plasmon polariton," Opt. Lett. **8**, 380–382 (1983).
19. J. C. Quail, J. G. Rako, and H. J. Simon, "Long-range surface-plasmon modes in silver and aluminum films," Opt. Lett. **8**, 377–379 (1983).
20. F. Z. Yang, G. W. Bradberry, and J. R. Sambles, "Long-range surface-mode supported by very thin silver films," Phys. Rev. Lett. **66**, 2030–2032 (1991).
21. J. Q. Xia, A. K. Jordan, and J. A. Kong, "Inverse-scattering view of modal structures in inhomogeneous optical waveguides," J. Opt. Soc. Am. A **9**, 740–748 (1992).
22. E. Anemogiannis, E. N. Glytsis, and T. K. Gaylord, "Determination of guided and leaky modes in lossless and lossy planar multilayer optical waveguides: reflection pole method and wavevector density method," J. Lightwave Technol. **17**, 929–941 (1999).
23. A. Otto, "Excitation of nonradiative surface plasma waves in silver by the method of frustrated total reflection," Z. Phys. **216**, 398–410 (1968).
24. B. Prade, J. Y. Vinet, and A. Mysyrowicz, "Guided optical waves in planar heterostructures with negative dielectric-constant," Phys. Rev. B **44**, 13556–13572 (1991).
25. E. N. Economou, "Surface plasmons in thin films," Phys. Rev. **182**, 539–554 (1969).
26. E. Anemogiannis and E. N. Glytsis, "Multilayer wave-guides —efficient numerical-analysis of general structures," J. Lightwave Technol. **10**, 1344–1351 (1992).
27. E. D. Palik, *Handbook of Optical Constants of Solids* (Academic, 1985).